Prospects for Localization of Gravitational Wave Transients by the Advanced LIGO and Advanced Virgo Observatories

The LIGO Scientific Collaboration and the Virgo Collaboration

January 28, 2013

Abstract

We present a possible observing scenario for the Advanced LIGO and Advanced Virgo gravitational wave detectors over the next decade, with the intention of providing information to the astronomy community to facilitate planning for multi-messenger astronomy with gravitational waves. We determine the expected sensitivity of the network to transient gravitational-wave signals, and study the capability of the network to determine the sky location of the source. We find that confident detections will likely require at least 2 detectors operating with ranges at least 100 Mpc, while ranges approaching 200 Mpc should give at least $\sim$1 detection per year even under pessimistic predictions of signal rates. Sky localisations depend on the geographical distribution of the detectors and their relative sensitivity, and can be as large as thousands of square degrees with only 2 sensitive detectors operating. Determining the sky position of a significant fraction of detected signals to areas of $5\,\mathrm{deg}^2$ to $20\,\mathrm{deg}^2$ will require at least 3 detectors of sensitivity within a factor of ~ 2 of each other and with a broad frequency bandwidth. Relocating one of the LIGO detectors to India would allow many gravitational-wave signals to be localized to a few square degrees by gravitational-wave observations alone.

1 Introduction

Advanced LIGO (aLIGO) [1] and Advanced Virgo (AdV) [2, 3] are kilometer-scale gravitational wave (GW) detectors that are expected to yield the first direct observations of gravitational waves. In this document we describe the currently projected schedule, sensitivity, and sky localization accuracy for the GW detector network. The purpose of this document is to provide information to the astronomy community to assist in the formulation of plans for the upcoming era of GW observations. In particular, we intend this document to provide the information required for assessing the features of programs for joint observation of GW events using electromagnetic, neutrino, or other observing facilities.

The full science of aLIGO and AdV is broad [4], and is not covered in this document. Instead, we concentrate on candidate GW transient signals. We place particular emphasis on the coalescence of neutron-star binary systems, which are the GW source with the most reliable predictions on the prospects of detection.

Although our collaborations have amassed a great deal of experience with GW detectors and analysis, it is still very difficult to make predictions for both improvements in search methods and for the rate of progress for detectors which are not yet fully installed or operational. *We stress that the scenarios of LIGO and Virgo detector sensitivity evolution and observing times given here represent our best estimates at present. They should not be considered as fixed or firm commitments.*

As the detectors' construction and commissioning progresses, we intend to release updates versions of this document.

2 Commissioning and Observing Phases

We divide the roadmap for the aLIGO and AdV observatories into three phases:

1. **Construction** includes the installation and testing of the detectors. This phase ends with *acceptance* of the detectors. Acceptance means that the interferometers can lock for periods of hours: light is resonant in the arms of the interferometer with *no guaranteed gravitational-wave sensitivity.* Construction will likely involve several short *engineering runs* with no expected astrophysical output as the detectors progress towards acceptance.

2. **Commissioning** will take the detectors from their configuration at acceptance through progressively better sensitivity to the ultimate second-generation detector sensitivity. Engineering and *science* runs in the commissioning phase will allow us to understand our detectors and analyses in an observational mode. It is expected that science runs will produce astrophysical results, including upper limits on the rate of sources and quite possibly the first detections of GWs. During this phase, exchange of GW candidates with partners outside the LSC and Virgo collaborations will be governed by memoranda of understanding (MOUs) [5].

3. **Observing** runs begin when the detectors are at or near full sensitivity. We anticipate that there will be a gradual transition from the commissioning to the observing phases. If it has not happened previously, the first few GW signals will be observed and the LSC and Virgo will be engaged in a long-term campaign to observe the GW sky. After the first four detections [5] we expect free exchange of GW event candidates with the astronomical community and the maturation of GW astronomy.

The progress in sensitivity as a function of time will affect the duration of the runs that we plan at any stage, as we strive to minimize the time to the first gravitational wave detection. Commissioning is a complex process which involves both scheduled improvements to the detectors and tackling unexpected new problems. While our experience makes us cautiously optimistic regarding the schedule for the advanced detectors, we note that we are targeting an order of magnitude improvement in sensitivity over a much wider frequency band. Consequently it is not possible to make concrete predictions for sensitivity as a function of time. We can, however, use our previous experience as a guide to plausible scenarios for the detector operational states that will allow us to reach the desired sensitivity. Unexpected problems could slow down the commissioning, but there is also the possibility that progress may happen faster than predicted here. As the detectors begin to be commissioned, information on the cost in time and benefit in sensitivity will become more apparent and drive the schedule of runs. More information on event rates, including the first detection, will also very likely change the schedule and duration of runs. In section 2.1 we present the commissioning plans for the aLIGO and AdV detectors. A summary of expected science runs is in section 2.2.

2.1 Commissioning and Observing Roadmap

The anticipated strain sensitivity evolution for aLIGO and AdV is shown in Fig. 1. A standard figure of merit for the sensitivity of an interferometer is the binary neutron star (BNS) *range*: the volume- and orientation-averaged distance at which a compact binary coalescence consisting of two

$1.4\,M_\odot$ neutron stars gives a matched filter signal-to-noise ratio of 8 in a single detector [6][1]. The BNS ranges for the various stages of aLIGO and AdV expected evolution are also provided in Fig. 1.

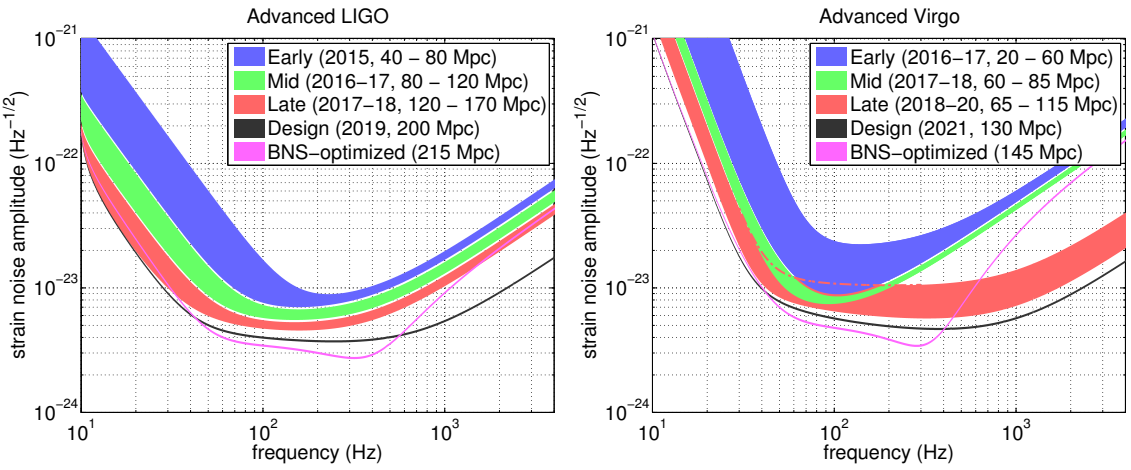

Figure 1: aLIGO (left) and AdV (right) target strain sensitivity as a function of frequency. The average distance to which binary neutron star (BNS) signals could be seen is given in Mpc. Current notions of the progression of sensitivity are given for early, middle, and late commissioning phases, as well as the final design sensitivity target and the BNS-optimized sensitivity. While both dates and sensitivity curves are subject to change, the overall progression represents our best current estimates.

The installation of aLIGO is well underway. The plan calls for three identical 4 km interferometers, referred to as H1, H2, and L1. In 2011, the LIGO Lab and IndIGO consortium in India proposed installing one of the aLIGO Hanford detectors, H2, at a new observatory in India (LIGO-India). As of early 2013 LIGO Laboratory, with NSF's permission, has begun preparing the H2 interferometer for shipment to India. Funding for the Indian portion of LIGO-India is in the final stages of consideration by the Indian government.

The first aLIGO science run is expected in 2015. It will be of order three months in duration, and will involve the H1 and L1 detectors (assuming H2 is placed in storage for LIGO-India). The detectors will *not* be at full design sensitivity; we anticipate a possible BNS range of 40 – 80 Mpc. Subsequent science runs will have increasing duration and sensitivity. We aim for a BNS range of 80 – 170 Mpc over 2016-18, with science runs of several months. Assuming that no unexpected obstacles are encountered, the aLIGO detectors are expected to achieve a 200 Mpc BNS range circa 2019. After the first observing runs, circa 2020, it may be possible to optimize the detector sensitivity for a specific class of astrophysical signals, such as BNSs. The BNS range may then become 215 Mpc. The sensitivity for each of these stages is shown in Fig. 1.

If the LIGO-India concept is pursued, the installation of the H2 detector in India will be delayed until construction of the LIGO-India Observatory is complete. The site development would start in 2014, with installation of the detector beginning in 2018. Assuming no unexpected problems, first runs are anticipated circa 2020 and design sensitivity at the same level as the H1 and L1 detectors

[1] Another often quoted number is the BNS *horizon*—the distance at which an optimally oriented and located BNS system would be observed with a signal to noise ratio of 8. The BNS horizon is a factor of 2.26 larger than the BNS range.

is anticipated for no earlier than 2022.

The commissioning timeline for AdV [3] is still being defined, but it is anticipated that in 2015 AdV may join the LIGO detectors in their first science run depending on the sensitivity attained. Following an early step with sensitivity corresponding to a BNS range of 20 – 60 Mpc, commissioning is expected to bring AdV to a 60 – 85 Mpc in 2017-18. A configuration upgrade at this point will allow the range to increase approximately 65 – 115 Mpc in 2018-20. The final design sensitivity, with a BNS range of 130 Mpc, is anticipated circa 2021. The corresponding BNS-optimised range would be 145 Mpc. The sensitivity curves for the various AdV configurations are shown in Fig. 1.

The GEO600 [7] detector will likely be operational in the early to middle phase of the AdV and aLIGO science runs, i.e. from 2015-2017. The sensitivity that potentially can be achieved by GEO in this timeframe is similar to the AdV sensitivity of the early and mid scenarios at frequencies around 1 kHz and above. Around 100 Hz GEO will be at least 10 times less sensitive than the early AdV and aLIGO detectors.

Japan has recently begun the construction of an advanced detector, KAGRA [8]. KAGRA is designed to have a BNS range greater than 100 Mpc at final sensitivity. While we do not consider KAGRA in this document, we note that the addition of KAGRA to the worldwide GW detector network will improve both sky coverage and localisation capabilities beyond those envisioned here.

2.2 Estimated observing schedule

Keeping in mind the mentioned important caveats about commissioning affecting the scheduling and length of science runs, the following is a plausible scenario for the operation of the LIGO-Virgo network over the next decade:

- 2015: A 3 month run with the two-detector H1L1 network at early aLIGO sensitivity (40 – 80 Mpc BNS range). Virgo in commissioning at $\sim$ 20 Mpc with a chance to join the run.
- 2016-17: A 6 month run with H1L1 at 80 – 120 Mpc and Virgo at 20 – 60 Mpc.
- 2017-18: A 9 month run with H1L1 at 120 – 170 Mpc and Virgo at 60 – 85 Mpc.
- 2019+: Three-detector network with H1L1 at full sensitivity of 200 Mpc and V1 at 65 – 115 Mpc.
- 2022+: Four-detector H1L1V1+LIGO-India network at full sensitivity (aLIGO at 200 Mpc, AdV at 130 Mpc).

The observational implications of this scenario are discussed in section 4.

3 Searches for gravitational-wave transients

Data from gravitational wave detectors are searched for many types of possible signals [4]. Here we focus on signals from compact binary coalescences (CBC), including BNS systems, and on generic transient or *burst* signals. See [9, 10, 11] for recent observational results from LIGO and Virgo for such systems.

The gravitational waveform from a binary neutron star coalescence is well known and matched filtering can be used to search for signals and measure the system parameters. For systems containing black holes, or in which the component spin is significant, uncertainties in the waveform model can reduce the sensitivity of the search. Searches for bursts make minimal assumptions on the signal morphology, using time-frequency decompositions to identify statistically significant

excess power transients in the data. Burst searches generally perform best for short-duration signals ($\lesssim$1 s); their astrophysical targets include core-collapse supernovae, magnetar flares, black hole binary coalescence, cosmic string cusps, and possibly as-yet-unknown systems.

In the era of advanced detectors, the LSC and Virgo will search in *near real-time* for CBC and burst signals for the purpose of rapidly identifying event candidates. A prompt notice of a potential GW transient by LIGO-Virgo might enable followup observations in the electromagnetic spectrum. A first followup program including low-latency analysis, event candidate selection, position reconstruction and the sending of alerts to several observing partners (optical, X-ray, and radio) was implemented and exercised during the 2009–2010 LIGO-Virgo science run [12, 13, 14]. Latencies of less than 1 hour were achieved and we expect to improve this in the advanced detector era. Increased detection confidence, improved sky localization, and identification of host galaxy and redshift are just some of the benefits of joint GW-electromagnetic observations. With this in mind, we focus on two points of particular relevance for followup of GW events: the source localization afforded by a GW network and the effect of signal significance (or false alarm rate) on the localization.

3.1 Localization

The aLIGO-AdV network will determine the sky position of a GW transient source mainly by triangulation using the observed time delays between sites [15, 16]. The single-site timing accuracy is approximately

$$\sigma_t = \frac{1}{2\pi\rho\sigma_f}\,, \tag{1}$$

where ρ is the signal-to-noise ratio in the given detector and σ_f is the effective bandwidth of the signal in the detector, typically of order 100 Hz. Thus a typical timing accuracy is on the order of 10^{-4} s (about 1/100 of the light travel time between sites). This sets the localization scale. There are, of course, many other issues that affect signal localization, for example: uncertainty in the emitted gravitational waveform, instrumental calibration accuracies, correlation of sky location with other binary parameters [17, 15, 18, 19] . While these will affect the localization details, the triangulation approach provides a good leading order estimate to localizations.

Source localization using only timing for a 2-site network yields an annulus on the sky; see Fig. 2. Additional information such as signal amplitude, spin, and precessional effects can sometimes resolve this to only parts of the annulus, but even then sources will only be localized to regions of hundreds to thousands of square degrees. For three detectors, the time delays restrict the source to two sky regions whose locations are mirror images in the plane formed by the three detectors. It is often possible to eliminate one of these regions by requiring consistent amplitudes in all detectors. For signals just above the detection threshold, this typically yields regions with areas of several tens of square degrees. If there is significant difference in sensitivity between detectors, the source is less well localized and we may be left with the majority of the annulus on the sky determined by the two most sensitive detectors. With four or more detectors, timing information alone is sufficient to localize to a single sky region, and the additional baselines help to limit the region to under 10 square degrees for some signals.

From (1), it follows that the *linear* size of the localization ellipse scales inversely with the signal to noise ratio (SNR) of the signal and the frequency bandwidth of the signal in the detector. For GWs which sweep across the band of the detector, such as binary merger signals, the effective bandwidth is ~ 100 Hz, determined by the most sensitive frequencies of the detector. For shorter transients the bandwidth σ_f depends on the specific signal. For example, GWs emitted by various

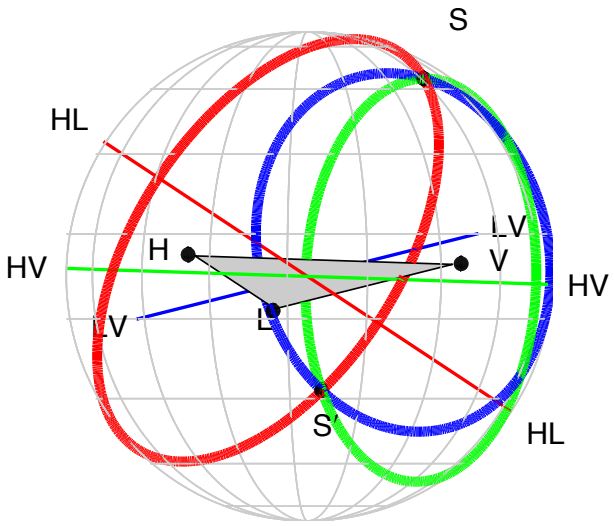

Figure 2: Source localization by triangulation for the aLIGO-AdV network. The locus of constant time delay (with associated timing uncertainty) between two detectors forms an annulus on the sky concentric about the baseline between the two sites. For three detectors, these annuli may intersect in two locations. One is centered on the true source direction, S, while the other (S') is its mirror image with respect to the geometrical plane passing through the three sites. For four or more detectors there is a unique intersection region of all of the annuli. Figure adapted from [20].

processes in core-collapse supernovae are anticipated to have bandwidths between 50-500 Hz [21, 22, 23, 24], largely independent of detector configuration. In addition, the sky localization region for generic burst signals may consist of multiple disconnected regions [25].

Finally, we note that some GW searches are triggered by electromagnetic observations, and in these cases localisation information is known *a priori*. For example, in GW searches triggered by gamma-ray bursts [10] the triggering satellite provides the localisation. The rapid identification of a GW counterpart to such a trigger could prompt further followups by other observatories. This is of particular relevance to binary mergers, which are considered the likely progenitors of most short gamma-ray bursts. It is therefore of utmost importance to have high-energy satellites operating during the advanced detector era.

Finally, it is also worth noting that all GW data are stored permanently, so that it is possible to perform retroactive analyses at any time.

3.2 Detection and False Alarm Rates

The rate of BNS coalescences is uncertain, but is currently predicted to lie between $10^{-8} - 10^{-5}\,\mathrm{Mpc}^{-3}\,\mathrm{y}^{-1}$ [26]. This corresponds to between 0.4 and 400 signals above SNR 8 per year of observation for a single aLIGO detector at final sensitivity [26]. The predicted observable rates for NS-BH and BBH are similar. Expected rates for other transient sources are lower and/or less well constrained.

The rate of triggers above a given SNR will depend critically upon the data quality of the advanced detectors; non-stationary transients or *glitches* will produce an elevated background of loud triggers. For low-mass binary coalescence searches, the waveforms are well modelled and signal consistency tests reduce the background to levels similar to those of Gaussian noise. For

burst sources which are not well modelled, or which spend only a short time in the detectors' sensitive band, it is more difficult to eliminate the effect of glitches.

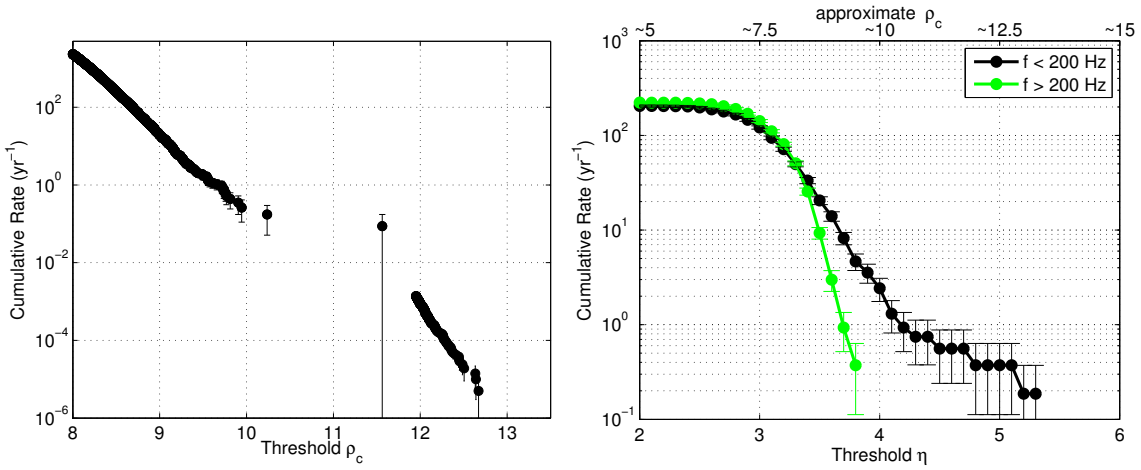

Figure 3: False alarm rate versus detection statistic for CBC and burst searches on 2009-2010 LIGO-Virgo data. Left: Cumulative rate of background events for the CBC search, as a function of the threshold ranking statistic ρ_c [9]. Right: Cumulative rate of background events for the burst search, as a function of the coherent network amplitude η [11]. In the large-amplitude limit η is related to the combined SNR by $\rho_c \sim \sqrt{2K}\eta$, where K is the number of detectors. The burst events are divided into two sets based on their central frequency.

Fig. 3 shows the noise background as a function of detection statistic for the low-mass binary coalescence and burst searches with the 2009-2010 LIGO-Virgo data [9, 11]. For binary mergers, the background rate decreases by a factor of ∼100 for every unit increase in combined SNR ρ_c, with no evidence of a tail even at low false alarm rates. Here, ρ_c is a combined, re-weighted SNR. The re-weighting is designed to reduce the SNR of glitches while leaving signals largely unaffected. Consequently, for a signal ρ_c is essentially the root-sum-square of the SNRs in the individual detectors.

We estimate a ρ_c threshold of 12 is required for a false rate of $\sim 10^{-2}\,\mathrm{y}^{-1}$ in aLIGO-AdV, where we have taken into account trials factors due to the increase (by at least an order of magnitude) in the number of template waveforms required to search the advanced detector data. In future sections, we quote results for this threshold. A combined SNR of 12 corresponds to a single detector SNR of 8.5 in each of two detectors or 7 in three detectors. At this threshold typically a quarter of detected signals can be localised (90% containment) to areas of $50\,\mathrm{deg}^2$ or less. For a background rate of $1\,\mathrm{y}^{-1}$ ($100\,\mathrm{y}^{-1}$) the threshold ρ_c decreases by about 10% (20%), the number of signals above threshold increases by about 30% (60%), and the area localization for these low-threshold signals is degraded by approximately 20% (40%).

Imperfections in the data can have a greater effect on the burst search. At frequencies above 200 Hz the rate of background events falls off steeply as a function of amplitude. At lower frequencies, however, the data often exhibit a significant tail of loud background events that are not removed by multi-detector consistency tests. While the extent of these tails varies, when present they typically begin at rates of approximately $1\,\mathrm{y}^{-1}$, hindering the confident detection of low-frequency gravitational-wave transients. Although the advanced detectors are designed with

many technical improvements, we must anticipate that burst searches will likely still have to deal with such tails in some cases, particularly at low frequencies. The unambiguous observation of an electromagnetic counterpart could increase the detection confidence in these cases.

A study [25] of the localisation capability of the burst search for the aLIGO-AdV network using a variety of waveform morphologies finds that at an SNR of $\rho_c \simeq 17$ (false rate of $\lesssim 0.1\,\mathrm{y}^{-1}$ from Fig. 3) the typical error box area for 50% (90%) containment is approximately $40\,\mathrm{deg}^2$ ($400\,\mathrm{deg}^2$). The median 50% containment area increases to $100\,\mathrm{deg}^2$ at $\rho_c \simeq 12$, and drops to approximately $16\,\mathrm{deg}^2$ at $\rho_c \simeq 25$. These results are broadly consistent with a study of two burst detection algorithms using real LIGO-Virgo data from 2009 [12], which shows that for signals near the nominal search threshold (coherent network amplitude $\eta \gtrsim 6$, corresponding $\rho_c \gtrsim 15$ [11]) median containment regions are typically between $30\,\mathrm{deg}^2$ and $200\,\mathrm{deg}^2$, dropping to approximately $10\,\mathrm{deg}^2$ at large amplitudes. See Fig. 4 for an example.

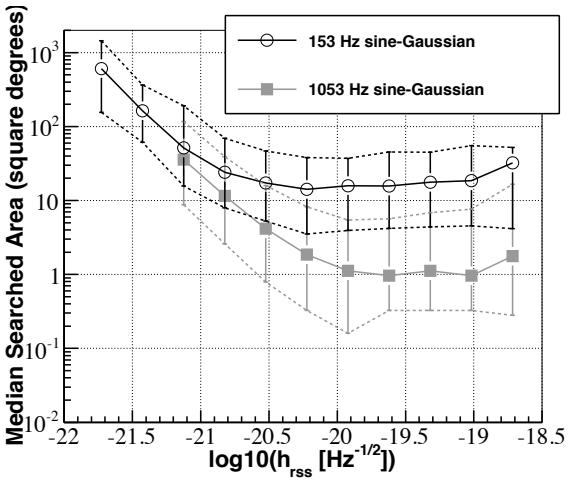

Figure 4: Plots of typical uncertainty region sizes for the burst search, as a function of GW strain amplitude at Earth, for two representative waveform types. The "searched area" is the area of the skymap with a likelihood value greater than the likelihood value at the true source location. The solid line with symbols represents the median (50%) performance, while the upper and lower dashed lines show the 75% and 25% quartile values. The detection threshold of $\eta \simeq 6$ corresponds to signal root-sum-square amplitudes of approximately $h_{\mathrm{rss}} \sim 0.5 \times 10^{-21}\,\mathrm{Hz}^{-1/2}$ to $\sim 2 \times 10^{-21}\,\mathrm{Hz}^{-1/2}$ [11], depending on signal frequency. Median uncertainty regions at these amplitudes are typically between $30\,\mathrm{deg}^2$ and $200\,\mathrm{deg}^2$. Figure from [12].

4 Observing Scenario

In this section we estimate the sensitivity, possible number of detections, and localization capability for each of the observing scenarios laid out in section 2.2. We discuss each future science run in turn and also summarize the results in Table 1.

We estimate the expected number of binary neutron star coalescence detections using both the lower and upper estimates on the BNS source rate density, $10^{-8} - 10^{-5}\,\mathrm{Mpc}^{-3}\,\mathrm{y}^{-1}$ [26]. Similar estimates may be made for neutron star – black hole (NS-BH) binaries using the fact that the

NS-BH range is approximately a factor of 2 larger[2] than the BNS range, though the uncertainty in the NS-BH source rate density is slightly larger [26]. We assume a nominal ρ_c threshold of 12, at which the expected false alarm rate is $10^{-2}\,\mathrm{y}^{-1}$. However, such a stringent threshold may not be appropriate for selecting candidates triggers for electromagnetic followup. For example, selecting CBC candidates at thresholds corresponding to a higher background rate of $1\,\mathrm{y}^{-1}$ ($100\,\mathrm{y}^{-1}$) would increase the number of true signals subject to electromagnetic followup by about 30% (60%). The area localization for these low-threshold signals is only fractionally worse than for the high-threshold population – by approximately 20% (40%). The localisation of NS-BH signals is expected to be similar to that of BNS signals.

For typical burst sources the GW waveform is not well known. However, the performance of burst searches is largely independent of the detailed waveform morphology [11], allowing us to quote an approximate sensitive range determined by the total energy E_{GW} emitted in GWs, the central frequency f_0 of the burst, and the single-detector SNR threshold [27]. In this document we quote ranges using $E_{\mathrm{GW}} = 10^{-2} M_\odot c^2$ and $f_0 = 150\,\mathrm{Hz}$. We note that $E_{\mathrm{GW}} = 10^{-2} M_\odot c^2$ is an optimistic value for GW emission by various processes (see e.g. [10]); for other values the distance reach scales as $E_{\mathrm{GW}}^{1/2}$. We use a single-detector SNR threshold of 8, corresponding to a typical $\rho_c \simeq 12$ and false alarm rates of $\sim 0.3\,\mathrm{y}^{-1}$. Due to the tail of the low-frequency background-rate-vs.-amplitude distribution in Fig. 3, we see that varying the selection threshold from a background of $0.1\,\mathrm{y}^{-1}$ ($\rho_c \gtrsim 15$) to even $3\,\mathrm{y}^{-1}$ ($\rho_c \gtrsim 10$) would increase the number of true signals selected for electromagnetic followup by a factor $(15/10)^3 \sim 3$, though the area localization for low-SNR bursts may be particularly challenging.

The run durations discussed below are in calendar time. Based on prior experience, we can reasonably expect a duty cycle of ∼80% for each instrument after a few science runs. Assuming downtime periods are uncorrelated among detectors, this means 50% coincidence time in a 3-detector network. Our estimates of expected number of detections account for these duty cycles. They also account for the uncertainty in the detector sensitive ranges as indicated in Fig. 1.

4.1 2015 run: aLIGO 40 – 80 Mpc, AdV 20 Mpc

This is envisioned as the first advanced detector science run, lasting three months. The aLIGO sensitivity is expected to be similar to the "early" curve in Fig. 1, with a BNS range of 40 – 80 Mpc and a burst range of 40 – 60 Mpc. The Virgo detector will be in commissioning, but may join the run with a ∼ 20 Mpc BNS range.

A three month run gives a BNS search volume[3] of $(0.4 - 3) \times 10^5\,\mathrm{Mpc}^3\,\mathrm{y}$ at the confident detection threshold of $\rho_c = 12$. We therefore expect $0.0004 - 3$ BNS detections. A detection is likely only if the most optimistic astrophysical rates hold.

With the 2-detector H1-L1 network any detected events would not be well localized, and even if AdV joins the run this will continue to be the case due to its lower sensitivity. Follow-up observations of a GW signal would therefore likely rely on localizations provided by another instrument, such as a gamma-ray burst satellite.

4.2 2016-17 run: aLIGO 80 – 120 Mpc, AdV 20 – 60 Mpc

This is envisioned to be a six month run with three detectors. The aLIGO performance is expected to be similar to the "mid" curve in Fig. 1, with a BNS range of 80 – 120 Mpc and a burst range of 60 – 75 Mpc. The AdV range may be similar to the "early" curve, approximately 20 – 60 Mpc for

[2] This assumes a black hole mass of $10\,M_\odot$.

[3] The search volume is $\frac{4}{3}\pi R^3 \times T$, where R is the range and T the observing time.

Epoch	Estimated Run Duration	Burst Range (Mpc) LIGO	Burst Range (Mpc) Virgo	BNS Range (Mpc) LIGO	BNS Range (Mpc) Virgo	Number of BNS Detections	% BNS Localized within $5\,\mathrm{deg}^2$	% BNS Localized within $20\,\mathrm{deg}^2$
2015	3 months	40 – 60	—	40 – 80	—	0.0004 - 3	-	-
2016–17	6 months	60 – 75	20 – 40	80 – 120	20 – 60	0.006 - 20	2	5-12
2017–18	9 months	75 – 90	40 – 50	120 – 170	60 – 85	0.04 - 100	1-2	10-12
2019+	(per year)	105	40 – 70	200	65 – 115	0.2 - 200	3-7	8-24
2022+ (India)	(per year)	105	80	200	130	0.4 - 400	17	48

Table 1: Summary of a plausible observing schedule, expected sensitivities, and source localization with the advanced LIGO and Virgo detectors, which will be strongly dependent on the detectors' commissioning progress. The burst ranges assume standard-candle emission of $10^{-2}M_{\odot}c^2$ in GWs at 150 Hz. The burst and binary neutron star (BNS) ranges and the BNS localizations reflect the uncertainty in the detector noise spectra shown in Fig. 1. The BNS detection numbers also account for the uncertainty in the BNS source rate density[26], and are computed assuming a false alarm rate of $10^{-2}\,\mathrm{y}^{-1}$. Burst localisations are expected to be broadly similar to those for BNS systems, but will vary depending on the signal bandwidth.

BNS and 20 – 40 Mpc for bursts. This gives a BNS search volume of $(0.6-2)\times10^6\,\mathrm{Mpc}^3\,\mathrm{y}$, and an expected number of $0.006-20$ BNS detections. Source localization for various points in the sky for CBC signals for the 3-detector network is illustrated in Fig. 5.

4.3 2017-18 run: aLIGO 120 – 170 Mpc, AdV 60 – 85 Mpc

This is envisioned to be a nine month run with three detectors. The aLIGO (AdV) sensitivity will be similar to the "late" ("mid") curve of Fig. 1, with BNS ranges of 120 – 170 Mpc and 60 – 85 Mpc respectively and burst ranges of 75 – 90 Mpc and 40 – 50 Mpc respectively. This gives a BNS search volume of $(3-10)\times10^6\,\mathrm{Mpc}^3\,\mathrm{y}$, and an expected $0.04-100$ BNS detections. Source localization for CBC signals is illustrated in Fig. 5. While the greater range compared to the 2016-17 run increases the expected number of detections, the detector bandwidths are marginally smaller. This slightly degrades the localization capability for a source at a fixed signal-to-noise ratio.

4.4 2019+ run: aLIGO 200 Mpc, AdV 65 – 115 Mpc

At this point we anticipate extended runs with the detectors at or near design sensitivity. The aLIGO detectors are expected to have a sensitivity curve similar to the "Final (2019)" curve of Fig. 1, while AdV may be operating similarly to the "late" curve. This gives a per-year BNS search volume of $2\times10^7\,\mathrm{Mpc}^3\,\mathrm{y}$, giving an expected (0.2 - 200) confident BNS detections annually. Source localization for CBC signals is illustrated in Fig. 5. The fraction of signals localised to areas of a few tens of square degrees is greatly increased compared to previous runs. This is due to the much larger detector bandwidths, particularly for AdV; see Fig. 1.

4.5 2022+ run: aLIGO (including India) 200 Mpc, AdV 130 Mpc

The four-site network incorporating LIGO-India at design sensitivity will have both improved sensitivity and better localization capabilities. The per-year BNS search volume increases to $4\times10^7\,\mathrm{Mpc}^3\,\mathrm{y}$, giving an expected $0.4-400$ BNS detections annually. Source localization is illustrated in Fig. 5. The addition of a fourth detector site allows for good source localisation over the whole sky.

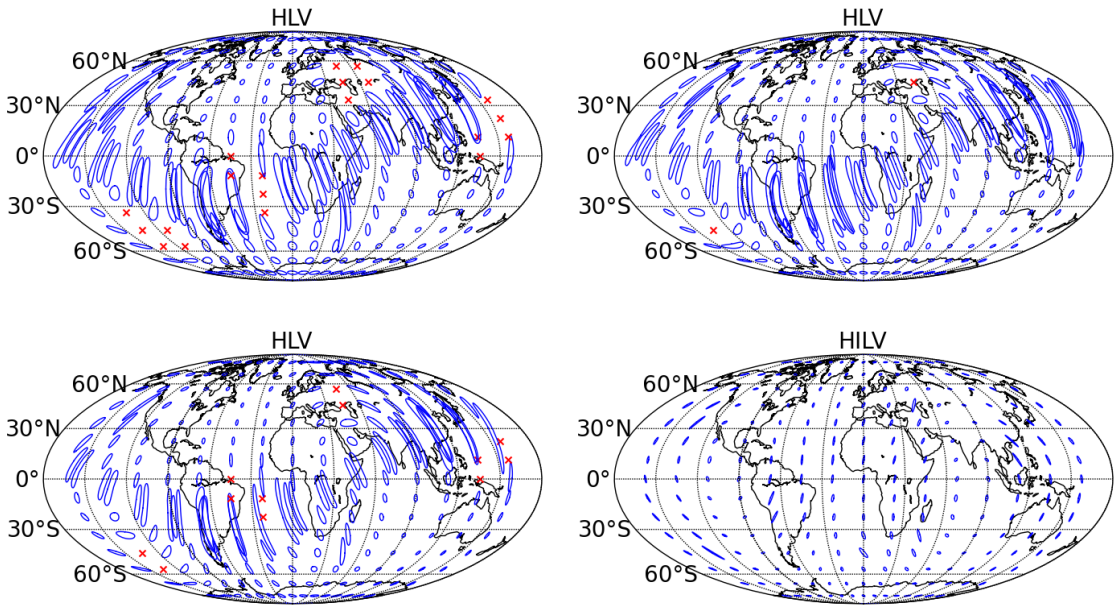

Figure 5: Network sensitivity and localization accuracy for face-on BNS systems with advanced detector networks. The ellipses show 90% confidence localization areas, and the red crosses show regions of the sky where the signal would not be confidently detected. The top two plots show the localization expected for a BNS system at 80 Mpc by the HLV network in the 2016-17 run (left) and 2017-18 run (right). The bottom two plots show the localization expected for a BNS system at 160 Mpc by the HLV network in the 2019+ run (left) and by the HILV network in 2022+ with all detectors at final design sensitivity (right). The inclusion of a fourth site in India provides good localization over the whole sky.

5 Conclusions

We have presented possible observing scenarios for the Advanced LIGO and Advanced Virgo network of gravitational wave detectors, with emphasis on the expected sensitivities and sky localization accuracies. This network is expected to begin operations in 2015. Before 2 or more detectors have an average range of at least 100 Mpc it is unlikely that a few months of observations will yield detections, unless the most optimistic astrophysical rates hold.

Electromagnetic followup of GW candidates *may* help confirm GW candidates that would not be confidently identified from GW observations alone. However, such follow-ups would need to deal with large position uncertainties, with areas of many tens to thousands of square degrees. This is likely to remain the situation until late in the decade. Optimizing the EM follow-up and source identification is an outstanding research topic.

For networks of more than 2 detectors with a range approaching 200 Mpc detections are expected with a year of observation based purely on GW data. Sky localization will continue to be poor until a third detector reaches a sensitivity within a factor of ~ 2 of the others and with a broad frequency bandwidth. In particular, with a four-site detector network at final design sensitivity, we may expect a significant fraction of GW signals to be localized to as well as a few square degrees by GW observations alone.

The purpose of this document is to assist the astronomy community in planning for multi-messenger astronomy with advanced gravitational-wave detectors. *While the scenarios described here are our best current projections, they will likely evolve as detector installation and commissioning progresses.* We will therefore update this document regularly.

The authors gratefully acknowledge the support of the United States National Science Foundation for the construction and operation of the LIGO Laboratory, the Science and Technology Facilities Council of the United Kingdom, the Max-Planck-Society, and the State of Niedersachsen/Germany for support of the construction and operation of the GEO600 detector, and the Italian Istituto Nazionale di Fisica Nucleare and the French Centre National de la Recherche Scientifique for the construction and operation of the Virgo detector. The authors also gratefully acknowledge the support of the research by these agencies and by the Australian Research Council, the International Science Linkages program of the Commonwealth of Australia, the Council of Scientific and Industrial Research of India, the Istituto Nazionale di Fisica Nucleare of Italy, the Spanish Ministerio de Educación y Ciencia, the Conselleria d'Economia Hisenda i Innovació of the Govern de les Illes Balears, the Foundation for Fundamental Research on Matter supported by the Netherlands Organisation for Scientific Research, the Polish Ministry of Science and Higher Education, the FOCUS Programme of Foundation for Polish Science, the Royal Society, the Scottish Funding Council, the Scottish Universities Physics Alliance, The National Aeronautics and Space Administration, the Carnegie Trust, the Leverhulme Trust, the David and Lucile Packard Foundation, the Research Corporation, and the Alfred P. Sloan Foundation. This document has been assigned LIGO Document number P1200087, Virgo Document number VIR-0288A-12.

References

[1] Harry, G. M. and the LIGO Scientific Collaboration. *Classical and Quantum Gravity* **27**(8), 084006 (2010).

[2] Acernese, F. et al. (2009). Virgo Technical Report VIR-0027A-09, https://tds.ego-gw.it/ql/?c=6589.

[3] Accadia, T. et al. (2012). Virgo Document VIR-0128A-12, https://tds.ego-gw.it/ql/?c=8940.

[4] Abadie, J. et al. (2012). LIGO Document number T1200286-v3, https://dcc.ligo.org/cgi-bin/private/DocDB/ShowDocument?docid=92545.

[5] Abadie, J. et al. (2012). LIGO Document number M1200055-v2, Virgo Document number VIR-0173A-12, https://dcc.ligo.org/cgi-bin/private/DocDB/ShowDocument?docid=89391.

[6] Finn, L. S. and Chernoff, D. F. *Phys. Rev. D* **47**, 2198–2219 Mar (1993). arXiv:9301003 [gr-qc].

[7] Lück, H. et al. *J. Phys.: Conf. Ser. 228 012012* (2010). J. Phys.: Conf. Ser. 228 012012.

[8] Somiya, K. *Classical and Quantum Gravity* **29**(12), 124007 (2012).

[9] Abadie, J. et al. *Phys. Rev. D* **85**, 082002 Apr (2012). arXiv:1111.7314.

[10] Abadie, J., Abbott, B. P., Abbott, R., et al. (2012). arXiv:1205.2216.

[11] Abadie, J. et al. *Phys. Rev. D* **85**, 122007 (2012). arXiv:1202.2788.

[12] Abadie, J. et al. *Astronomy & Astrophysics* **539**, A124 (2012).

[13] Abadie, J. et al. *Astronomy & Astrophysics* **541**, A155 (2012).

[14] Evans, P. et al. (2012). arXiv:1205.1124.

[15] Fairhurst, S. *New J.Phys.* **11**, 123006 (2009). arXiv:0908.2356.

[16] Fairhurst, S. *Class.Quant.Grav.* **28**, 105021 (2011). arXiv:1010.6192.

[17] Vitale, S. and Zanolin, M. (2010).

[18] Vitale, S., Del Pozzo, W., Li, T. G., Van Den Broeck, C., Mandel, I., et al. *Phys.Rev.* **D85**, 064034 (2012).

[19] Nissanke, S., Sievers, J., Dalal, N., and Holz, D. *Astrophys.J.* **739**, 99 (2011).

[20] Chatterji, S., Lazzarini, A., Stein, L., Sutton, P. J., Searle, A., et al. *Phys.Rev.* **D74**, 082005 (2006).

[21] Dimmelmeier, H., Ott, C. D., Marek, A., and Janka, H.-T. *Phys. Rev. D* **78**(6), 064056 September (2008).

[22] Ott, C. D. *Class. Quantum Grav.* **29**, 063001 (2009).

[23] Yakunin, K. N., Marronetti, P., Mezzacappa, A., Bruenn, S. W., Lee, C.-T., Chertkow, M. A., Hix, W. R., Blondin, J. M., Lentz, E. J., Bronson Messer, O. E., and Yoshida, S. *Classical and Quantum Gravity* **27**(19), 194005 October (2010).

[24] Ott, C. D., Reisswig, C., Schnetter, E., O'Connor, E., Sperhake, U., Löffler, F., Diener, P., Abdikamalov, E., Hawke, I., and Burrows, A. *Physical Review Letters* **106**(16), 161103 April (2011).

[25] Klimenko, S., Vedovato, G., Drago, M., Mazzolo, G., Mitselmakher, G., Pankow, C., Prodi, G., Re, V., Salemi, F., and Yakushin, I. *Physical Review D* **83**(10), 102001 May (2011). arXiv:1101.5408.

[26] Abadie, J. et al. *Classical and Quantum Gravity* **27**(17), 173001 September (2010). arXiv:1003.2480.

[27] Sutton, P. J. (2010). LIGO Document number LIGO-P1000041-v2, https://dcc.ligo.org/cgi-bin/private/DocDB/ShowDocument?docid=10614.